Investigation of a Large-Scale Mode of Ocean–Atmosphere Variability and Its Relation to Tropical Pacific Sea Surface Temperature Anomalies

BRUCE T. ANDERSON

Department of Geography, Boston University, Boston, Massachusetts

4 August 2003 and 29 March 2004

ABSTRACT

By examining the linearly coupled atmospheric and oceanic signals related to interannual variability in sea surface temperatures and upper-air wind fields, a hemispheric-scale ocean–atmosphere teleconnection mode is isolated that is significantly correlated with equatorial Pacific SSTs 12 months later. The interannual component of this teleconnection mode is related to a basin-scale dipole in the upper-air wind fields stretching across the extratropical Pacific, with additional anomalies extending from the eastern tropical Pacific over North America and into the Atlantic basin. In addition, it is related to variability in the SST field with warm anomalies found over the tropical/subtropical western Pacific as well as the equatorial eastern Pacific; also, there are related cold anomalies over the extratropical central North Pacific that extend down into the central subtropical/tropical Pacific. Diagnostic studies investigating the ocean–atmosphere structure for this mode of variability indicate that the large-scale variations in the upper-air circulation patterns are associated with anomalous equatorward propagation of transient and stationary wave activity over the North Pacific. In addition, they are characterized by vertical circulation patterns over both the subtropical and extratropical Pacific, which are collocated with variations in surface pressure and wind stress fields over the central subtropical and tropical North Pacific. Previous research has shown that modifications of these two fields are significantly related to the evolution of equatorial Pacific SSTs and may provide the dynamic mechanism whereby the ocean–atmosphere teleconnection mode described here influences the development of the ENSO system. This influence appears to be related to a modification of the basin-scale heat content over the central and eastern tropical Pacific; however, significant discussion is provided concerning alternative hypotheses.

1. Introduction

Sea surface temperature (SST) anomalies have been shown to act as an effective, large-scale boundary forcing of the climate, principally during hemispheric winter (Kumar and Hoerling 1998; Zheng et al. 2000; Shukla et al. 2000). As an example, the El Niño–Southern Oscillation (ENSO) phenomenon, which entails the relative warming of the sea surface temperatures (SSTs) over the eastern equatorial Pacific, provides significant forcing of the overlying atmosphere, resulting in hemispheric-scale circulation changes (e.g., Trenberth et al. 1998; Alexander et al. 2002). Numerous additional modes of atmospheric variability have been identified through various statistical techniques (e.g., see Horel and Wallace 1981; Mo and Livezey 1986; Barnston and Livezey 1987; Trenberth and Hurrell 1994), some of which are related to independently derived large-scale interannual-to-multidecadal structures in both Pacific and Atlantic basins (Enfield and Mestas-Nunez 1999). However, many of these atmospheric teleconnection patterns, both forced and unforced, are to a large extent interrelated (e.g., Barnston and Livezey 1987; Thompson and Wallace 1998). In an attempt to better isolate well-correlated ocean–atmosphere teleconnection features, we perform a statistical analysis between modes of upper-air wind and SST variability. In doing so, we isolate a mode of ocean–atmosphere variability related to the development of ENSO-like SST anomalies in the tropical Pacific. The paper investigates the ocean–atmosphere structure associated with this mode of variability, its relation to previously identified modes of atmospheric variability, as well as its possible influence on the evolution of the ENSO system.

2. Data

The principal dataset used in this investigation is the reanalysis product from the National Centers for Environmental Prediction–National Center for Atmospheric Research (NCEP–NCAR, see acknowledgments). Details about this dataset, including its physics, dynamics, and numerical and computational methods, are discussed in Kalnay et al. (1996); a description of the reanalysis SST dataset can be found in Hurrell and Tren-

Corresponding author address: Bruce T. Anderson, Department of Geography, Boston University, 675 Commonwealth Ave., Boston, MA 02215-1401.
E-mail: brucea@bu.edu

berth (1999). In this study we will examine the seasonal mean fields for January–February–March (JFM) for the years 1948–2000. All data are detrended prior to analysis in order to reduce low-frequency correlations. Also, it should be noted that all data are archived after incorporation of the Television Infrared Observation Satellite (TIROS) Operational Vertical Sounder (TOVS) data processing correction, which previously had introduced large-scale errors from 1998 to 2000 (more information available online at http://wesley.wwb.noaa.gov/tovsproblem). In addition to the reanalyzed data, we also utilize the Climate Prediction Center (CPC) Merged Analysis of Precipitation (CMAP) data (Xie and Arkin 1997), which is an observationally based merged satellite–gauge dataset at 2.5° × 2.5° resolution spanning 1979–2003. For characterization of the ocean state, we archive the observational analysis from the Joint Environmental Data Analysis Center (JEDAC), which uses an optimal interpolation procedure to produce 5° × 2.5° gridded values of temperature, mixed-layer depth, and heat content (vertically integrated from the surface to 400 m; White 1995; W. B. White 2003, personal communication), from 1955 to 2000. As with the reanalysis data, we will examine the seasonal mean fields for JFM unless otherwise noted.

We also include time series data for various oceanic and atmospheric indices, taken principally from the National Oceanic and Atmospheric Administration–Cooperative Institute for Research in Environmental Sciences (NOAA–CIRES) Climate Diagnostics Center (see acknowledgments for data availability). The primary observational index is the Niño-3.4 index, which is defined as the area-averaged SST anomalies between 5°N–5°S and 170°–120°W and is designed to capture variability in the SST field over the equatorial Pacific. Other indices include the Western Pacific (WP) and Trans-Niño Index (TNI); references for each are provided in the text.

3. Results

To detect and isolate the major large-scale atmospheric/oceanic patterns, the NCEP–NCAR reanalysis data are used to compute empirical orthogonal functions (EOFs) for the area-weighted, boreal wintertime (JFM) sea surface temperature anomalies from 15°S to 55°N, as well as for the contemporaneous 250-mb zonal wind anomalies from 0° to 60°N, which characterize large-scale and free-atmospheric dynamics associated with major steering patterns (Arkin 1982; Trenberth et al. 1998). The EOFs for the SSTs are limited to 55°N due to spurious values seen in the far northern Atlantic and Pacific (Hurrell and Trenberth 1999); in addition, they are extended south to 15°S in order to encompass the full anomalies associated with equatorial Pacific SST forcing. The 250-mb zonal wind anomalies are limited to the winter hemisphere (i.e., the Northern Hemisphere) because of the strong response of the hemispheric winter climate system to SST variations (Kumar and Hoerling 1998; Zheng et al. 2000; Shukla et al. 2000). To analyze the correlation between spatial and temporal patterns within the SST and analyzed wind fields, we perform a canonical correlation analysis (CCA: Bretherton et al. 1992). This technique attempts to minimize the variance between a subset of the zonal wind and SST EOF time series in order to produce a set of canonical factor (CF) time series that isolate the highest correlated modes of variability within the two datasets; the subset of EOFs used for the CCA is limited to the first nine for the zonal wind field and the first seven for the SST field, which explain 79% (77%) of the Northern Hemispheric JFM zonal wind (SST) variability.

Overall, both spatial and temporal patterns for the first canonical factor (CF1) are related to the El Niño–Southern Oscillation (not shown). The correlation between the two canonical factor time series is 0.97. The SST map for the first canonical factor (explaining 33% of the total equatorial/Northern Hemisphere JFM variability) is characterized by strong warming in the equatorial Pacific with additional cooling over the western equatorial and subtropical Pacific. The first zonal-wind pattern (which explains 23% of the total Northern Hemisphere wintertime variability) contains a tropical–extratropical pattern over the central Pacific, characterized by an extension and southward shift of the jet stream over subtropical North America, as well as teleconnection features over the higher latitudes of North America and the western Atlantic.

Figure 1 shows the temporal and spatial patterns for the second canonical factor (CF2). The correlation between the two time series is 0.83. For the spatial fields, we calculate the regression of the near-global SST and zonal wind anomalies against the respective time series in order to better capture the large-scale extent of the anomalies under consideration; all regression values are quantitatively the same as those found in the reduced domains used to calculate the original EOF and CF time series. The SST map for the second canonical factor (representing 9% of the total equatorial/Northern Hemisphere variability) is related to warming over the eastern and far-western tropical Pacific, with additional warming over the western and central extratropical Pacific; cooling is found in a horseshoe pattern over the high-latitude northern Pacific, extending down into the central tropical Pacific. The upper-air wind pattern (representing 7% of the total Northern Hemisphere zonal wind variability) is characterized by a dipole feature over the extratropical Pacific basin. In addition there is a negative equatorial anomaly over the eastern Pacific with wavelike features extending into North America and the extratropical Atlantic sector.

It should be noted that despite the SST anomalies in the eastern equatorial Pacific, this mode of variability is not related to the concurrent ENSO state ($r = 0.13/0.12$ for the Niño-3.4 and SST/zonal wind time series)

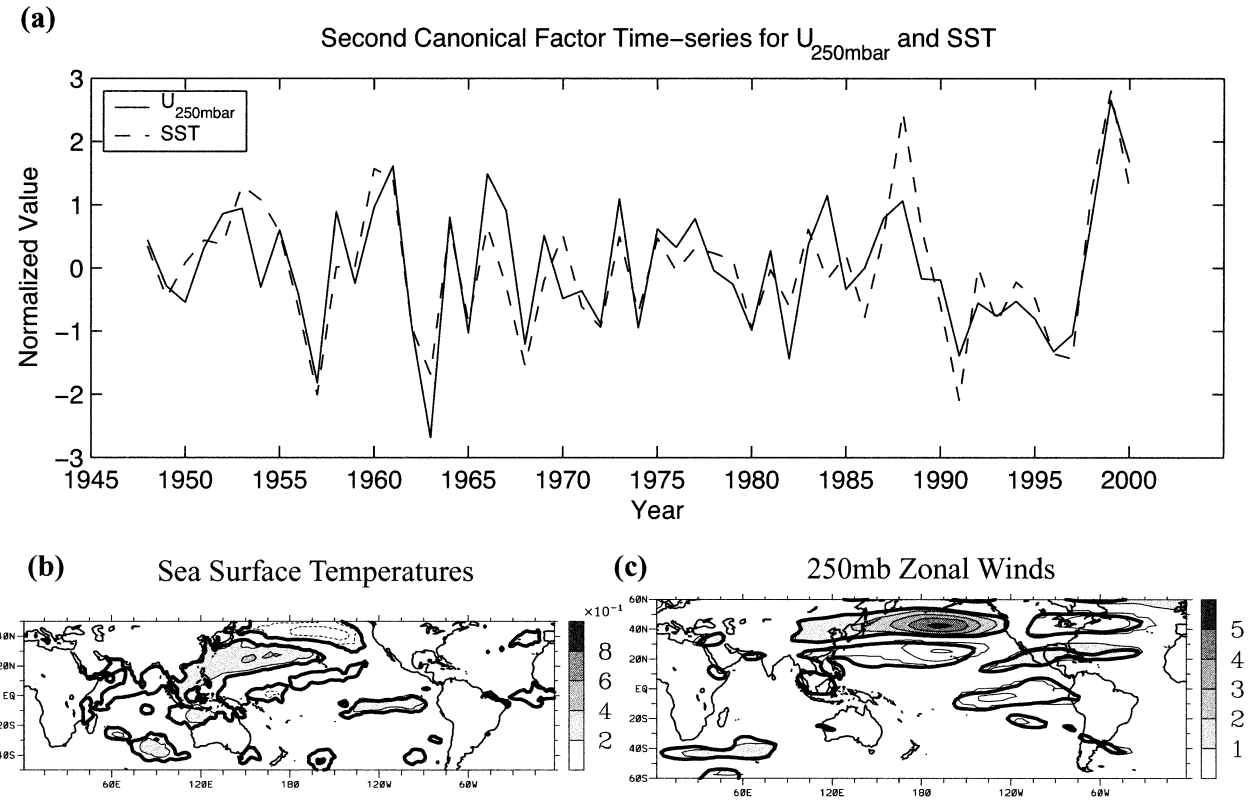

FIG. 1. (a) Normalized time series for second canonical factor of JFM 250-mb zonal wind anomalies (solid line) and SST anomalies (dashed line) taken from the NCEP–NCAR reanalysis. The time series are normalized such that they have unit variance. Therefore, the associated geographic patterns in Figs. 3b,c represent characteristic anomalies in the SST and zonal wind fields. (b) CF2 pattern of SST anomalies. Contour interval is 0.2 K; minimum contour is ±0.2 K. Positive values are shaded; negative values are dashed. Thick black line represents regions with correlation values greater than ±0.27 (approximately 95% confidence limit). (c) CF2 pattern of 250-mb zonal wind anomalies. Contour interval is 1 m s^{-1}; minimum contour is ±1 m s^{-1}. Positive values are shaded; negative values are dashed. Thick black line represents regions with correlation values greater than ±0.27.

nor the ENSO state from the previous year ($r = 0.20/0.09$ for the JFM Niño-3.4 and the lagged JFM SST/zonal wind time series). Instead, the SST structure is qualitatively similar to a previously identified non-ENSO tropical Pacific SST index (the Trans-Niño Index; Trenberth and Tepaniak 2001) and shows some temporal correlation with the index itself ($r = 0.30$ and 0.26 for the SST and zonal wind time series, respectively). This correspondence is particularly true for the period 1978–2000 when the correlations rise to $r = 0.54$ and 0.59 (for the SST and zonal wind time series, respectively); prior to this period, however, the correlations are actually of opposite sign ($r = -0.20$ and -0.27 for the period 1958–1977), suggesting that the two time series may represent separate, but intermittently related, phenomena.

In comparing the CF2 mode of variability with numerous other indices of Northern Hemisphere climate variability, it appears to be most strongly correlated with the ''Western Pacific'' pattern isolated within the Northern Hemisphere 700-mb height field (Barnston and Livezey 1987 $r = 0.47$ and 0.56 for the SST and zonal wind time series, respectively). A similar WP-type pattern has also been isolated by applying a single value decomposition (SVD) to the covariance matrix between the Northern Hemisphere wintertime 500-mb heights and global surface temperatures (including land surface temperatures, Koide and Kodera 1999), suggesting that the pattern isolated via CCA is not a statistical artifact of the technique itself. We also obtain similar SST and upper-air zonal wind structures when we perform a maximum covariance analysis (MCA) by applying a single-value decomposition to the combined SST–zonal wind anomaly matrix (after normalizing, area-weighting, and adjusting for the number of grid points—not shown); however, when using the MCA technique, the ocean–atmosphere mode of variability discussed here is the fourth principal component due to the small amount of total variance explained within the two respective fields. This rearrangement highlights a subtle, but useful, difference between the MCA and CCA techniques. Whereas MCA orders the isolated components based upon the total fraction of squared covariance explained, the CCA technique orders factors based upon correlation values between the respective time series and can thereby iso-

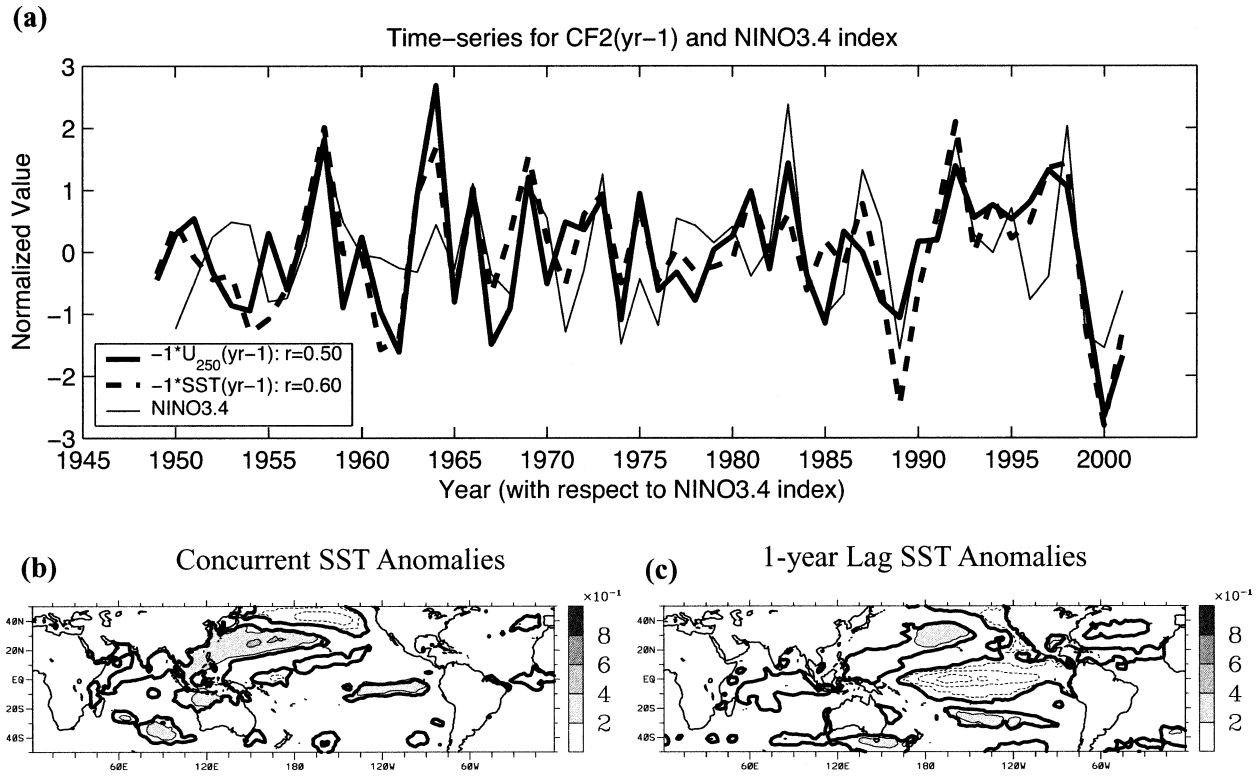

FIG. 2. (a) Normalized time series for the CF2 of JFM 250-mb zonal wind anomalies (thick solid line) and SST anomalies (thick dashed line), both multiplied by −1 and lagged by 1 yr. Therefore, values represent those 1 yr prior to that shown on the *x* axis. Also shown is the normalized Niño-3.4 index for the given year (thin solid line). The time series are normalized such that they have unit variance. (b) JFM SST anomalies correlated with the CF2 SST time series for the concurrent year. Contour interval is 0.2 K; minimum contour is ±0.2 K. Positive values are shaded; negative values are dashed. Thick black line represents regions with correlation values greater than ±0.27 (approximately 95% confidence limit). (c) As in Fig. 3b except for JFM SST anomalies correlated with the CF2 SST time series from the preceding year.

late modes that may explain a lesser amount of variance but are more highly correlated.

As mentioned, this mode of variability only explains a small fraction of the total Northern Hemisphere zonal wind variance. However, this mode of variability may still be an important component of the large-scale climate system in that it may play a role in the subsequent evolution of the ENSO phenomena. In particular, the lagged correlation between the second canonical factor time series and the following year's first canonical factor time series (representative of ocean–atmosphere variability associated with ENSO) indicates that the CF2 time series has a moderate, but significant, negative lead correlation with the ENSO-related CF1 signal ($r = -0.56$ and -0.64 for the zonal wind CF1/CF2 time series and SST CF1/CF2 time series, respectively). In addition, Fig. 2 demonstrates that the two CF2 time series are also correlated with observed equatorial SST anomalies the following winter ($r = -0.50$ and -0.60 for the zonal wind and SST CF2/Niño-3.4 index). The negative correlation between the CF2 time series and the lagged Niño-3.4 index (as well as the anomalies associated with the concurrent and lagged SST fields) indicates that the correlation is not due to persistence in the equatorial SST signal; for instance, a warm water tropical Pacific anomaly associated with the CF2 field correlates with a La Niña event (i.e., cold water anomaly) in the SST fields the next year.

These findings indicate that there may be a dynamic mechanism whereby this mode of variability in the ocean–atmosphere, although small, can in fact influence the full ENSO state the following year. As mentioned, a similar upper-air pattern, related to the Western Pacific mode, has been found by applying a SVD to the covariance matrix between the Northern Hemisphere wintertime 500-mb height patterns and global surface temperatures (Koide and Kodera 1999). This WP-type pattern, in turn, has been related to wintertime SST anomalies in the South China Sea, (Ose 2000), which have also been shown to have a lead relationship with ENSO anomalies the following year (Ose et al. 1997). However, the lead correlation between the wintertime WP itself and the following wintertime Niño-3.4 index is only −0.35. Still, these results further suggest that the ocean–atmosphere pattern isolated here may be related to the evolution of the ENSO system. In addition, it is important to note that although the correlation between the TNI (which also has a lead relation with ENSO;

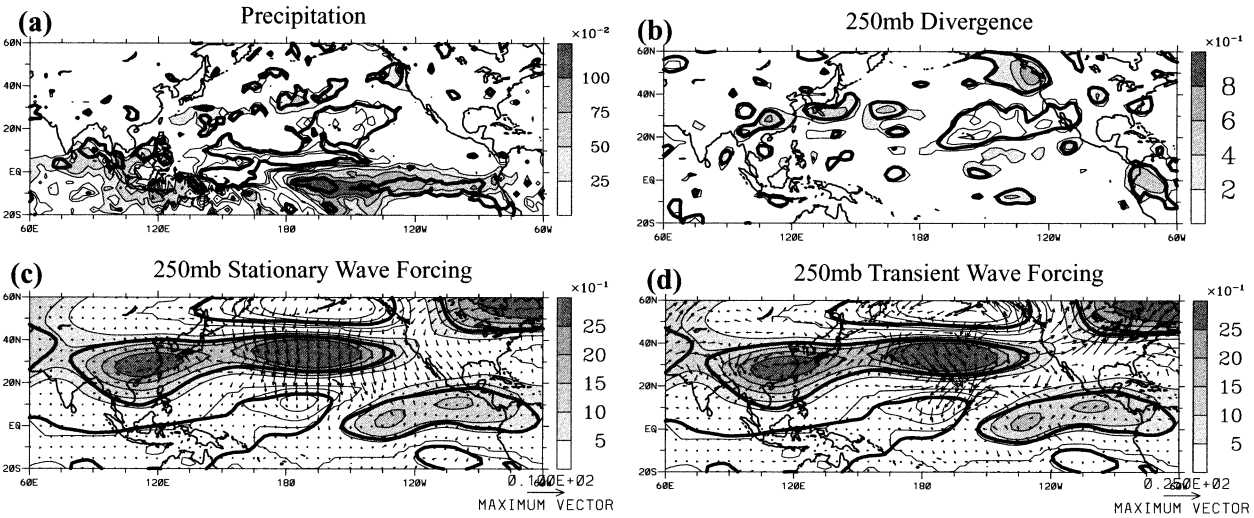

FIG. 3. (a) JFM precipitation anomalies derived from the CMAP dataset regressed against the concurrent JFM CF2 time series of 250-mb zonal winds. Regression performed for 1979–2000; see text for details. Positive values are shaded; negative values are contoured. Shading interval is 0.25 mm day^{-1}; minimum contour is $\pm$0.25 mm day^{-1}. Thick black line represents regions with correlation values greater than $\pm$0.45 (approximately the 95th percentile). (b) JFM seasonal-mean 250-mb divergence values regressed against the concurrent JFM CF2 time series of 250-mb zonal winds. Regression performed for 1950–2000; see text for details. Positive values are shaded; negative values are contoured. Shading interval is 0.2×10^{-6} s^{-1}; minimum contour is $\pm 0.2 \times 10^{-6}$ s^{-1}. In all subsequent panels, thick black line represents regions with correlation values greater than $\pm$0.275 (approximately the 95th percentile). (c) As in Fig. 3b except for JFM 250-mb streamfunction. Also shown are 250-mb $\mathbf{F}_s$ vectors regressed against the concurrent JFM CF2 time series of 250-mb zonal winds; see text for details. Shading interval is 0.5×10^6 m^2 s^{-1}; minimum contour is $\pm 0.5 \times 10^6$ m^2 s^{-1}. Reference vector is 10 m^2 s^{-2}. (d) As in Fig. 3c except for 250-mb $\mathbf{E}$ vectors; see text for details. Shading interval for streamfunction is 0.5×10^6 m^2 s^{-1}; minimum contour is $\pm 0.5 \times 10^6$ m^2 s^{-1}. Reference vector is 25 m^2 s^{-2}.

Trenberth and Tepaniak 2001) and the CF2 time series breaks down prior to 1978, there is still a similar correlation between the CF2 time series and the lagged equatorial Pacific SSTs prior to this time period, albeit weaker ($r = -0.48/-0.35$ for the lagged Niño-3.4 and SST–zonal wind time series from 1950 to 1977; $r = -0.68/-0.64$ for the time series from 1978 to 2000), suggesting that the lagged correlation between ENSO and the CF2 mode of ocean–atmosphere variability holds both before and after the climate regime shift in 1978 (Trenberth 1990).

To better diagnose the atmospheric structure associated with this mode of variability, we correlate the second canonical factor time series of 250-mb zonal winds with atmospheric dynamic and thermodynamic fields (Fig. 3). For this figure, both seasonal and ENSO-related signals are linearly removed (the former by removing the climatological seasonal mean; the latter by removing the linearly correlated ENSO signal from the seasonal anomaly field); this is done in order to better capture signals in regions where overall variance is dominated by ENSO activity. Overall, the second canonical factor is significantly correlated with observed precipitation anomalies over the central and eastern equatorial Pacific. In addition, it is negatively correlated with precipitation over the Hawaiian Islands as well as to the east of Indonesia (although the latter is not significant at the 95% level). The related 250-mb divergence field, seen in Fig. 3b, contains significant anomalous convergence over the central subtropical North Pacific, collocated with the negative precipitation anomalies in this region. Significant anomalous divergence is found over southern China and the western subtropical North Pacific, as well as the midlatitude northwest Pacific. There is also significant anomalous divergence at 150 mb over the central equatorial Pacific in the region of maximum precipitation anomalies (not shown). However, there is no significant divergence/convergence over Indonesia, in agreement with the weakly correlated precipitation values seen over this region. Associated with these upper-air divergence patterns are seasonal-mean 250-mb Rossby wave source anomalies, defined by Sardeshmukh and Hoskins (1988), which indicate significant Rossby wave sources over the central subtropical and extratropical Pacific, collocated with anomalies in the divergence fields (not shown). In addition, there is a large (but weakly significant) anticyclonic vorticity source over the Himalayas extending over the Yellow Sea, collocated with divergence in this region.

While both the divergence and Rossby wave–source terms suggest forcing by subtropical/extratropical seasonal-mean potential vorticity anomalies, it has also been shown that both stationary and transient wave activity play an important role in maintaining seasonal-mean patterns (e.g., Hoerling et al. 1992). To capture propagation associated with anomalous stationary wave activity, the seasonal mean 250-mb $\mathbf{F}_s$ vectors, as defined in Plumb (1985), are estimated. These vectors,

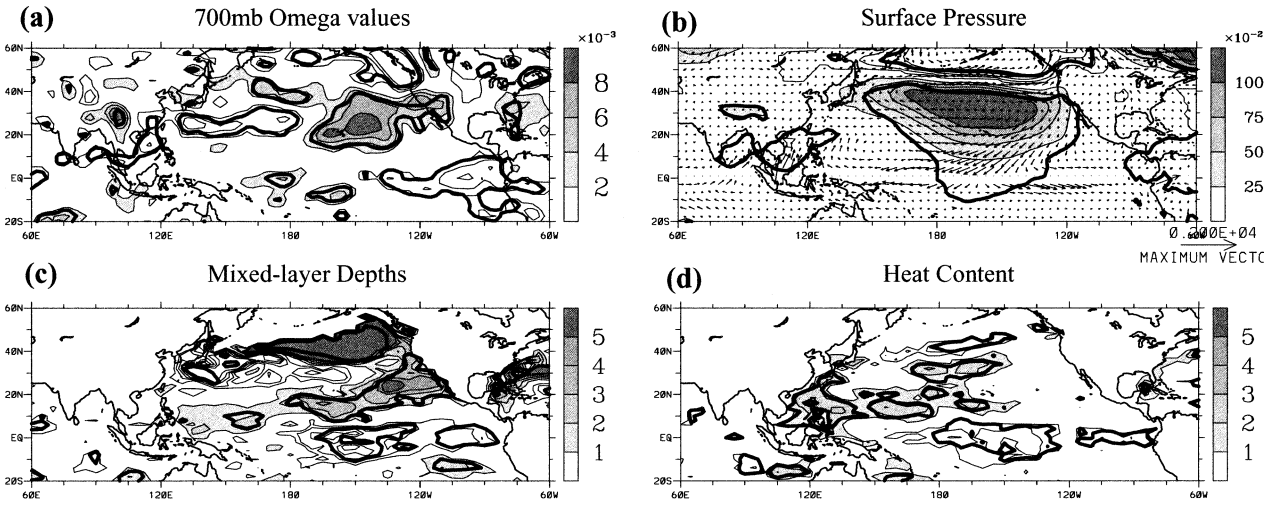

FIG. 4. (a) JFM seasonal-mean 700-mb omega values regressed against the concurrent JFM CF2 time series of 250-mb zonal winds. Regression performed for 1950–2000; see text for details. The omega values are equal to vertical motion in pressure coordinates at the given level such that negative values indicate upward motion. Positive values are shaded; negative values are dashed. Shading interval is 0.002 Pa s^{-1}; minimum contour is ± 0.002 Pa s^{-1}. In all subsequent panels, thick black line represents regions with correlation values greater than ± 0.275 (approximately the 95th percentile). (b) As in Fig. 4a except for JFM surface pressures. Also shown are the wind stress vectors regressed against the concurrent JFM CF2 time series of 250-mb zonal winds and divided by the magnitude of the Coriolis parameter; see text for details. Shading interval is 0.25 mb; minimum contour is ± 0.25 mb. Reference vector is 2000 kg m^{-1} s^{-1}. (c) As in Fig. 4a except for analyzed observations of ocean mixed-layer depths. Shading interval is 1 m; minimum contour is ± 1 m. (d) Same as in Fig. 4a except for analyzed observations of ocean heat content. Shading interval is 1×10^8 J m^{-2}; minimum contour is $\pm 1 \times 10^8$ J m^{-2}.

whose horizontal components point approximately in the direction of the plane-wave group velocity, are computed using the full streamfunction gridpoint values for each season; the seasonal-mean vector anomalies are then regressed against the second canonical factor time series for zonal winds. Results (Fig. 3c) indicate a significant anomalous equatorward propagation associated with stationary waves, similar to results found for the establishment of WP-type anomalies (Kodera 1998). In addition, this propagation appears to be related to significant wavelike features in the 250-mb streamfunction anomalies themselves, suggesting that the large-scale variations in the upper-air circulation, captured by the zonal wind fields, are partly related to changes in stationary wave forcing. We also estimate the wave propagation associated with transient activity by computing the seasonal mean 250-mb **E** vectors, defined as in Matthews and Kiladis (1999), to better parallel the transient group velocity (relative to the mean velocity) associated with barotropic disturbances (see Plumb 1986); these vectors are calculated using daily anomalies of zonal and meridional winds, taken with respect to the seasonal-mean gridpoint values for the given year. The seasonal-mean vectors are regressed against the second CF time series of zonal winds and are plotted in Fig. 3d, again with the 250-mb streamfunction regression map. Over the central Pacific, there is further indication of anomalous equatorward propagation, along with enhanced northeastward propagation from the eastern Pacific into the region of anomalous high pressure over North America; this divergence of wave activity is related to a convergence of momentum that may help reinforce the stationary circulation anomalies (as in Lorenz and Hartmann 2003).

Further investigation of ''composite'' maps of stationary wave activity associated with positive/negative values in the second canonical factor times series of zonal winds indicate that, for positive values of the time series, the full fields show an eastward extension of the western Pacific streamfunction dipole and a flattening of the ridge over the eastern midlatitude Pacific (not shown). This eastward extension of the circulation patterns, and its relationship to phase changes in ENSO, is in agreement with the findings of Ose et al. (1997), which suggested that biennial variations (as opposed to low-frequency variations) in ENSO are related in part to a similar eastward shift in the basin-scale wind anomalies. Associated with this more zonal orientation of the upper-air circulation is an enhancement of the climatological equatorward propagation of stationary wave energy over the central subtropical Pacific (Plumb 1985) and a decrease in northward propagation to the higher latitudes; in addition, there also appears to be a decrease in stationary wave activity over North America and the Atlantic basin.

To see how the anomalous circulation may impact the subsequent evolution of the ENSO system, the second canonical factor time series is next correlated with low-level ocean and atmosphere anomalies (Fig. 4). As seen previously, the establishment and maintenance of the upper-air circulation anomalies (see Figs. 1c and 3c,d) is related to large-scale vertical circulation features, as

indicated by the significant anomalous convergence situated over the Hawaiian Islands (Fig. 3b). This convergence is collocated with significant changes in the underlying vertical velocity field, as can be seen in the 700-mb omega values (Fig. 4a). These changes in the vertical circulation are in turn collocated with variations in the low-level surface pressure patterns and wind stress anomalies (Fig. 4b). The former fields indicate a basinwide high pressure anomaly over the subtropical Pacific. In addition, wind stress anomalies (divided by the local Coriolis parameter to provide estimates of Ekman mass transport) indicate strong, anticyclonic anomalous wind forcing extending into the Tropics with equatorial easterly anomalies from Indonesia to the date line. Previous research has demonstrated that subtropical and tropical wind anomalies over the western and central Pacific can influence the evolution of the observed and simulated ENSO system (Kidson 1975; Rasmusson and Carpenter 1982; van Loon and Shea 1985; Li 1997; Weisberg and Wang 1997; B. Wang et al. 1999; C. Wang et al. 1999; Chan and Xu 2000; Vimont et al. 2003a,b). In particular, the sea level pressure anomalies in Fig. 4b are in agreement with modes of sea level pressure variability, found in both model simulations and reanalysis data, that have been shown to be significantly correlated with mature ENSO events 12–15 months later (Vimont et al. 2003a,b). In addition, a previously identified sea level pressure index in the region of the Hawaiian Islands (defined as the SLP anomalies area averaged over 10°–25°N, 140°–175°W; Anderson 2003), designed to capture similar variability in the subtropical central Pacific sea level pressure field preceding ENSO events, is well correlated with the CF2 time series ($r = 0.70$ and $r = 0.73$ for the upper-air zonal wind and SST time series, respectively). Together, these results indicate that the SST and upper-air zonal wind patterns associated with the second CF and the independently derived precursor sea level pressure patterns (Vimont et al. 2003b; Anderson 2003) may represent a coherent mode of ocean–atmosphere variability that can influence the subsequent evolution of the ENSO system through their modification of the trade wind regime (further discussion can be found in section 5).

To see how the wind stress anomalies associated with the subtropical high pressure center are related to the ocean structure, Fig. 4c shows the mixed-layer depth anomalies regressed against the second canonical factor time series for upper-air zonal winds. This figure indicates that the large wind stress anomalies over the central equatorial Pacific are collocated with a decrease in the mixed-layer depth. The structure of the mixed-layer depth is in dynamic agreement with the wind stress curl (not shown), which suggests strong equatorial upwelling from 150°W to 180° (associated with equatorial easterly anomalies) and off-equatorial (5°–10°N) upwelling from 120°–150°W (associated with the north–south gradient in both the tropical westerly anomalies and the Coriolis parameter); additional equatorial upwelling may also result from the divergence of the wind stress field near 150°W. In addition to the decrease in mixed-layer depths in the equatorial central Pacific, there are deeper mixed-layer depths in the tropical North Pacific (10°–20°N) and shallower mixed-layer depths in the subtropical North Pacific (~30°N), all in agreement with the curl of the wind stress. Interestingly, although there are upwelling favorable winds off the coast of California, there is actually a deepening of the mixed-layer in this region, possibly due to advection and redistribution of large-scale heat flux anomalies as in Di Lorenzo et al. (2004). Finally, there is a significant deepening of the mixed-layer in the central and eastern extratropical Pacific, most likely due to enhanced mixing associated with the anomalously strong surface westerlies. Importantly, the shoaling of the mixed-layer depths in the central tropical Pacific is collocated with significant decreases in the ocean heat content (Fig. 4d). It is this decrease in ocean heat content that in turn may produce the well-correlated lagged tropical sea surface temperature anomalies associated with the second CF mode of ocean–atmosphere variability isolated here (McPhaden 2003).

4. Summary

The relationship between changes in January–March upper-air patterns and interannual variability in underlying SSTs is investigated using output from 50-plus years of NCEP–NCAR reanalysis data. Results indicate that within the analyzed system there is a mode of tropical/extratropical ocean–atmosphere variability that is significantly correlated with the development of SST anomalies in the central/eastern tropical Pacific 1 yr later. This mode of variability is related to variability in the upper-air winds across the Pacific basin with teleconnection features over eastern North America and the subtropical and extratropical Atlantic. In addition, there are also SST anomalies over the eastern equatorial Pacific, in the ENSO region, and throughout the western and central tropical/extratropical North Pacific associated with this mode of variability. Correspondence with previous results relating subtropical SLP anomalies to the development of the ENSO system (Vimont et al. 2003b; Anderson 2003) suggests that this mode of SST/upper-air variability may influence the evolution of the ENSO system by modulating the subtropical high pressure patterns found over the central Pacific and thereby establish subtropical trade wind anomalies that are conducive to initiating ENSO events the following year. Our results suggest they do so by altering the basin-scale subsurface heat content across the central and eastern tropical Pacific. However, we do not suggest that this is the sole mechanism whereby ENSO events can be initiated; there are many additional mechanisms capable of initiating ENSO events, which are then maintained by dynamics internal to the equatorial atmo-

sphere–ocean system (e.g., see Neelin et al. 1998 and below).

5. Discussion

This note is designed to describe a mode of large-scale ocean–atmosphere variability during the boreal winter that appears to influence the evolution of the ENSO system over the following year, possibly through its modulation of the subtropical surface pressures and trade winds. It is still unclear from this research, however, what dynamic/thermodynamic role the trade winds play in the development of the ENSO system. From research presented above, we attempt to argue that the influence occurs during the boreal winter, during which time the overlying wind anomalies produce subsurface temperature and heat content anomalies in the central and eastern tropical Pacific that are conducive to initiating overlying surface temperature anomalies the following spring (e.g., Jin 1997; Meinen and McPhaden 2000; McPhaden 2003). In particular, these results are in agreement with studies that indicate boreal winter heat content anomalies lead the SST signal and result in the initiation of SST anomalies after the boreal spring ''predictability barrier'' (McPhaden 2003). However, it is important to note that various other hypotheses have also been proposed for the initiation of equatorial Pacific SST anomalies by subtropical/extratropical ocean–atmosphere processes. For instance, recent studies (Vimont et al. 2003a,b) suggest that Northern Hemisphere wintertime sea level pressure variability over the subtropics/extratropics, very similar to that described here, can initiate underlying subtropical/tropical SST anomalies, which then persist until the summer; during the summer period these SSTs can subsequently force the overlying atmosphere, resulting in zonal wind stress anomalies that are conducive to initiating and maintaining the Kelvin wave structure necessary for ENSO variability in the tropical Pacific. This mechanism is diagnosed in climate models (Vimont et al. 2001, 2003a) and appears to be active in the observed system as well (Vimont et al. 2003b). Here we suggest that the influence of this mode of variability upon the evolution of the ENSO system is not only felt during the following boreal summer, but also concurrently during the boreal winter through modifications of the underlying basin-scale subsurface structure. Alternatively, other researchers have suggested that similar anomalous pressure and wind patterns found over the central and eastern subtropical Pacific during boreal winter may instead initiate subsurface temperature anomalies that propagate westward as Rossby waves (Chan and Xu 2000), then reflect at the western boundary and propagate eastward within the thermocline; these anomalies may shoal in the central and eastern Pacific approximately 6 months later and initiate the onset of an ENSO event.

It is also possible that surface heat flux anomalies associated with the anomalous winds may force a boreal spring basin-scale SST structure that in turn is optimal for intrinsic ENSO growth over the following 7–9 months (as envisioned by Penland 1996). Finally, the initiation of ENSO events may be due to concurrent wind anomalies over the western tropical Pacific, either in the form of mean tropical winds or transient westerly wind bursts, which can lead to a change in the thermocline depth in the western equatorial Pacific that propagates eastward, resulting in an ENSO event in the central Pacific (Li 1997; McPhaden 1999; Wang 2001). However Yu et al. (2003) show that westerly wind bursts are not effective if the atmosphere over the western tropical Pacific is not properly preconditioned to allow for extensive fetch into the open ocean; other researchers indicate that the ocean heat content over the central Pacific also has to be preconditioned such that Kelvin waves initiated by the westerly wind bursts can effectively alter the surface temperature structure (Perigaud and Cassou 2000; Fedorov 2002). In these scenarios, the large-scale surface circulations associated with the mode of ocean–atmosphere variability discussed here may serve to precondition both the atmospheric structure (see Fig. 4b) as well as the underlying subsurface ocean structure (see Figs. 4c,d), thereby allowing other forcing mechanisms, such as westerly wind bursts, to become more effective. Needless to say, much more extensive diagnosis of the dynamic and thermodynamic response of the ocean to the overlying wind fields associated with this mode of ocean–atmosphere variability is still needed.

Another uncertainty concerns where the ''forcing'' for the large-scale anomalous upper-level atmospheric circulation resides. For instance, as mentioned, a similar WP-type pattern has been related to wintertime SST anomalies in the South China Sea (Ose 2000), suggesting that at least part of the analyzed atmospheric variability isolated here may be related to forcing from underlying SST anomalies in the tropical Indo–Pacific region. However, other researchers have suggested this WP-like pattern may instead be related to early winter circulation features over Eurasia (Kodera 1998). Alternatively, it may be a response to anomalous SSTs in the Kuroshio region (Yulaeva et al. 2001), which are similar to those found in Fig. 1b, or internal atmospheric variability as suggested by Vimont et al. (2001), which is sustained by interactions between the mean circulations and stationary/transient wave activity (e.g., Chang et al. 2002). Research designed to delineate the source of this mode of ocean–atmosphere variability is presently being conducted.

A final question that arises is whether this mode of ocean–atmosphere variability is simply related to the early stages of ENSO variability and is in turn a response to ENSO's intrinsic evolution as opposed to an initiation of that evolution. Studies of the evolution of the SST signature for the ENSO system indicate that significant SST anomalies do not typically occur until April–May prior to JFM ENSO events (Harrison and

Larkin 1998; Larkin and Harrison 2002), in agreement with the concept of a spring ''predictability barrier'' associated with a lack of forecast skill for ENSO-related SST evolution across the boreal spring (Webster and Yang 1992). In comparison, the mode of SST/upper-air variability discussed here is found in the preceding January–March period; as suggested above, during this time it may serve to initiate boreal winter heat-content anomalies and/or boreal spring optimal initial SST structures, both of which appear to overcome the ''spring predictability barrier'' associated with ENSO-related SST evolution (Penland 1996; McPhaden 2003). Alternatively, the mode of variability discussed here may be related to the intrinsic evolution of the subsurface anomalies preceding mature ENSO events (e.g., Jin 1997; Li 1997), although how these subsurface anomalies may influence the hemispheric-scale upper-air atmospheric anomalies seen in Fig. 1c is unclear; if so, however, the results presented here suggest that the mode of variability is capturing the associated large-scale ocean–atmosphere anomalies outside the tropical Pacific, which can further influence the evolution of the system. Finally, it is possible that the mode of variability discussed here is related to the atmospheric evolution of the ENSO system associated with previous June–September sea level pressure and wind stress anomalies over the western subtropical South Pacific and equatorial Indian Ocean, both of which have been shown to lead mature JFM ENSO events by approximately 18 months (Trenberth 1976; Rasmusson and Carpenter 1982; van Loon and Shea 1985, 1987; Clarke and van Gorder 2003). Correlation of the CF2 time series with eastward equatorial wind stress anomalies (as defined in Clarke and van Gorder 2003) indicates that there are no significant anomalies in the equatorial Indian Ocean preceding the JFM CF2 time series (not shown). However, normalized SLP anomalies for June–August, area averaged over 20°–42.5°S, 129.5°–160°E (representing the core of western subtropical South Pacific SLP regression anomalies 18 months prior to JFM ENSO events—see Fig. 1b of van Loon and Shea 1987), are moderately correlated with the following JFM CF2 zonal wind/SST time series ($r = 0.35/0.41$, respectively). This result is similar to that found in Anderson (2003) in which the subtropical South Pacific SLP index described above and a subtropical North Pacific SLP index situated over Hawaii were found to be correlated ($r = 0.35$); in that paper it was suggested that the two indices may represent separate, but possibly related, modes of subtropical variability that, when occurring in succession, have a strong forcing influence upon the tropical Pacific ocean–atmosphere system.

Acknowledgments. We thank Kingtse Mo for her insightful comments on drafts of this paper. NCEP–NCAR reanalysis data were provided by the NOAA–CIRES Climate Diagnostics Center, Boulder, Colorado, from their Web site (http://www.cdc.noaa.gov). Climate indices were provided by NOAA–CIRES Climate Diagnostics Center, Boulder, Colorado, from their Web site (http://www.cdc.noaa.gov/ClimateIndices/index.html).

REFERENCES

Alexander, M. A., I. Bladé, M. Newman, J. R. Lanzante, N.-C. Lau, and J. D. Scott, 2002: The atmospheric bridge: The influence of ENSO teleconnections on air–sea interaction over the global oceans. *J. Climate,* **15,** 2205–2231.

Anderson, B. T., 2003: Tropical Pacific sea-surface temperatures and preceding sea level pressure anomalies in the subtropical North Pacific. *J. Geophys. Res.,* **108,** 4732, doi:10.1029/2003JD003805.

Arkin, P. A., 1982: The relationship between interannual variability in the 200 mb tropical wind field and the Southern Oscillation. *Mon. Wea. Rev.,* **110,** 1393–1404.

Barnston, A. G., and R. E. Livezey, 1987: Classification, seasonality and persistence of low-frequency atmospheric circulation patterns. *Mon. Wea. Rev.,* **115,** 1083–1126.

Bretherton, C. S., C. Smith, and J. M. Wallace, 1992: An intercomparison of methods for finding coupled patterns in climate data. *J. Climate,* **5,** 541–560.

Chan, J. C. L., and J. J. Xu, 2000: Physical mechanisms responsible for the transition from a warm to a cold state of the El Niño–Southern Oscillation. *J. Climate,* **13,** 2056–2071.

Chang, E. K. M., S. Lee, and K. Swanson, 2002: Storm track dynamics. *J. Climate,* **15,** 2163–2183.

Clarke, A. J., and S. van Gorder, 2003: Improving El Niño prediction using a space–time integration of Indo–Pacific winds and equatorial Pacific upper ocean heat content. *Geophys. Res. Lett.,* **30,** 1399, doi:10.1029/2002GL016673.

Di Lorenzo, E., A. J. Miller, N. Schneider, and J. C. McWilliams, 2004: The warming of the California current system: Dynamics and ecosystem implications. *J. Phys. Oceanogr.,* in press.

Enfield, D. B., and A. M. Mestas-Nunez, 1999: Multiscale variabilities in global sea surface temperatures and their relationships with tropospheric climate patterns. *J. Climate,* **12,** 2719–2733.

Fedorov, A. V., 2002: The response of the coupled tropical ocean–atmosphere to westerly wind bursts. *Quart. J. Roy. Meteor. Soc.,* **128,** 1–23.

Harrison, D. E., and N. K. Larkin, 1998: El Niño–Southern Oscillation sea surface temperature and wind anomalies, 1946–1993. *Rev. Geophys.,* **36,** 353–399.

Hoerling, M. P., M. L. Blackmon, and M. Ting, 1992: Simulating the atmospheric response to the 1985–1987 El Niño cycle. *J. Climate,* **5,** 669–682.

Horel, J. D., and J. M. Wallace, 1981: Planetary-scale atmospheric phenomena associated with the Southern Oscillation. *Mon. Wea. Rev.,* **109,** 813–829.

Hurrell, J. W., and K. E. Trenberth, 1999: Global sea surface temperature analyses: Multiple problems and their implications for climate analysis, modeling, and reanalysis. *Bull. Amer. Meteor. Soc.,* **80,** 2661–2678.

Jin, F.-F., 1997: An equatorial ocean recharge paradigm for ENSO. Part I: Conceptual model. *J. Atmos. Sci.,* **54,** 811–829.

Kalnay, E., and Coauthors, 1996: The NCEP/NCAR 40-Year Reanalysis Project. *Bull. Amer. Meteor. Soc.,* **77,** 437–471.

Kidson, J. W., 1975: Tropical eigenvector analysis and the Southern Oscillation. *Mon. Wea. Rev.,* **103,** 187–196.

Kodera, K., 1998: Consideration of the origin of the different midlatitude atmospheric responses among El Niño events. *J. Meteor. Soc. Japan,* **76,** 347–361.

Koide, H., and K. Kodera, 1999: A SVD analysis between the winter NH 500-hPa height and surface temperature fields. *J. Meteor. Soc. Japan,* **77,** 47–61.

Kumar, A., and M. P. Hoerling, 1998: Annual cycle of Pacific–North American seasonal predictability associated with different phases of ENSO. *J. Climate,* **11,** 3295–3308.

Larkin, N. K., and D. E. Harrison, 2002: ENSO warm (El Niño) and cold (La Niña) event life cycles: Ocean surface anomaly patterns, their symmetries, asymmetries, and implications. *J. Climate,* **15,** 1118–1140.

Li, T., 1997: Phase transition of the El Niño–Southern Oscillation: A stationary SST mode. *J. Atmos. Sci.,* **54,** 2872–2887.

Lorenz, D. J., and D. L. Hartmann, 2003: Eddy-zonal flow feedback in the Northern Hemisphere winter. *J. Climate,* **16,** 1212–1227.

Matthews, A. J., and G. N. Kiladis, 1999: Interactions between ENSO, transient circulation, and tropical convection over the Pacific. *J. Climate,* **12,** 3062–3086.

McPhaden, M. J., 1999: Genesis and evolution of the 1997–98 El Niño. *Science,* **283,** 950–954.

——, 2003: Tropical Pacific Ocean heat content variations and ENSO persistence barriers. *Geophys. Res. Lett.,* **30,** 1480, doi:10.1029/2003GL016872.

Meinen, C. S., and M. J. McPhaden, 2000: Observations of warm water volume changes in the equatorial Pacific and their relationship to El Niño and La Niña. *J. Climate,* **13,** 3551–3559.

Mo, K. C., and R. E. Livezey, 1986: Tropical–extratropical geopotential height teleconnections during the Northern Hemisphere winter. *Mon. Wea. Rev.,* **114,** 2488–2515.

Neelin, J. D., D. S. Battisti, A. C. Hirst, F.-F. Jin, Y. Wakata, T. Yamagata, and S. E. Zebiak, 1998: ENSO theory. *J. Geophys. Res.,* **103,** 14 261–14 290.

Ose, T., 2000: A biennially oscillating sea surface temperature and the western Pacific pattern. *J. Meteor. Soc. Japan,* **78,** 93–99.

——, Y. K. Song, and A. Kitoh, 1997: Sea surface temperature in the South China Sea—An index for the Asian monsoon and ENSO system. *J. Meteor. Soc. Japan,* **75,** 1091–1107.

Penland, C., 1996: A stochastic model of IndoPacific sea surface temperature anomalies. *Physica D,* **98,** 534–558.

Perigaud, C. M., and C. Cassou, 2000: Importance of oceanic decadal trends and westerly wind bursts for forecasting El Niño. *Geophys. Res. Lett.,* **27,** 389–392.

Plumb, R. A., 1985: On the three-dimensional propagation of stationary waves. *J. Atmos. Sci.,* **42,** 217–229.

——, 1986: Three-dimensional propagation of transient quasi-geostrophic eddies and its relationship with the eddy forcing of the time–mean flow. *J. Atmos. Sci.,* **43,** 1657–1678.

Rasmusson, E. M., and T. H. Carpenter, 1982: Variations in tropical sea surface temperature and surface wind fields associated with the Southern Oscillation/El Niño. *Mon. Wea. Rev.,* **110,** 354–384.

Sardeshmukh, P. D., and B. J. Hoskins, 1988: The generation of global rotational flow by steady idealized tropical divergence. *J. Atmos. Sci.,* **45,** 1228–1251.

Shukla, J., and Coauthors, 2000: Dynamical seasonal prediction. *Bull. Amer. Meteor. Soc.,* **81,** 2593–2606.

Thompson, D. W. J., and J. M. Wallace, 1998: The Arctic Oscillation signature in the wintertime geopotential height and temperature fields. *Geophys. Res. Lett.,* **25,** 1297–1300.

Trenberth, K. E., 1976: Spatial and temporal variations of the Southern Oscillation. *Quart. J. Roy. Meteor. Soc.,* **102,** 639–653.

——, 1990: Recent observed interdecadal climate changes in the Northern Hemisphere. *Bull. Amer. Meteor. Soc.,* **71,** 988–993.

——, and J. W. Hurrell, 1994: Decadal atmosphere–ocean variations in the Pacific. *Climate Dyn.,* **9,** 303–319.

——, and D. P. Tepaniak, 2001: Indices of El Niño evolution. *J. Climate,* **14,** 1697–1701.

——, G. W. Branstator, D. Karoly, A. Kumar, N.-C. Lau, and C. Ropelewski, 1998: Progress during TOGA in understanding and modeling global teleconnections associated with tropical sea surface temperatures. *J. Geophys. Res.,* **103** (C7), 14 291–14 324.

van Loon, H. L., and D. J. Shea, 1985: The Southern Oscillation. Part IV: The precursors south of 15°S to the extremes of the oscillation. *Mon. Wea. Rev.,* **113,** 2063–2074.

——, and ——, 1987: The Southern Oscillation. Part VI: Anomalies of sea level pressure on the Southern Hemisphere and of Pacific sea surface temperature during the development of a warm event. *Mon. Wea. Rev.,* **115,** 370–379.

Vimont, D. J., S. Battisti, and A. C. Hirst, 2001: Footprinting: A seasonal connection between the tropics and mid-latitudes. *Geophys. Res. Lett.,* **28,** 3923–3926.

——, ——, and ——, 2003a: The seasonal footprinting mechanism in the CSIRO general circulation models. *J. Climate,* **16,** 2653–2667.

——, J. M. Wallace, and S. Battisti, 2003b: The seasonal footprinting mechanism in the Pacific: Implications for ENSO. *J. Climate,* **16,** 2668–2675.

Wang, B., R. Wu, and R. Lukas, 1999: Roles of the western North Pacific wind variation in thermocline adjustment and ENSO phase transition. *J. Meteor. Soc. Japan,* **77,** 1–16.

Wang, C., 2001: A unified oscillator model for the El Niño–Southern Oscillation. *J. Climate,* **14,** 98–115.

——, R. H. Weisberg, and J. I. Virmani, 1999: Western Pacific interannual variability associated with the El Niño–Southern Oscillation. *J. Geophys. Res.,* **104,** 5131–5149.

Webster, P. J., and S. Yang, 1992: Monsoon and ENSO: Selectively interactive systems. *Quart. J. Roy. Meteor. Soc.,* **118,** 877–926.

Weisberg, R. H., and C. Z. Wang, 1997: A western Pacific oscillator paradigm for the El Niño–Southern Oscillation. *Geophys. Res. Lett.,* **24,** 779–782.

White, W. B., 1995: Design of a global observing system for gyre-scale upper ocean temperature variability. *Progress in Oceanography,* Vol. 36, Pergamon, 169–217.

Xie, P., and P. A. Arkin, 1997: Global precipitation: A 17-year monthly analysis based on gauge observations, satellite estimates, and numerical model outputs. *Bull. Amer. Meteor. Soc.,* **78,** 2539–2558.

Yu, L., R. A. Weller, and W. T. Liu, 2003: Case analysis of a role of ENSO in regulating the generation of westerly wind bursts in the western equatorial Pacific. *J. Geophys. Res.,* **108,** 3128, doi: 10.1029/2002JC001498.

Yulaeva, E., N. Schneider, D. W. Pierce, and T. P. Barnett, 2001: Modeling of North Pacific climate variability forced by oceanic heat flux anomalies. *J. Climate,* **14,** 4027–4046.

Zheng, X. G., H. Nakamura, and J. A. Renwick, 2000: Potential predictability of seasonal means based on monthly time series of meteorological variables. *J. Climate,* **13,** 2591–2604.